ChemComm

COMMUNICATION

View Article Online
View Journal | View Issue

Cite this: *Chem. Commun.*, 2016, 52, 13807

Received 19th September 2016,
Accepted 1st November 2016

DOI: 10.1039/c6cc07611d

www.rsc.org/chemcomm



# Solution processable formation of a few nanometer thick-disordered overlayer on the surface of open-ended $TiO_2$ nanotubes†

Soon Woo Kwon,‡[a] Ming Ma,‡[a] Myung Jin Jeong,[b] Kan Zhang,[b] Sung June Kim[c] and Jong Hyeok Park*[b]

**Herein, we designed vertically aligned $TiO_2$ nanotube arrays, in which a very thin disordered overlayer approximately a few nm thick was formed *via* a room-temperature solution process. At the optimal overlayer thickness, the $TiO_2$ nanotube arrays yielded a photocurrent density of up to ~1.75 mA $cm^{-2}$ at 1.23 V *vs.* RHE, approximately twice that of the pristine one.**

Hydrogen is a clean energy source with a variety of applications, such as heating systems, aircraft and vehicles. With the development of production methods, solar energy takes on a new role as an assistant power resource. Photoelectrochemical (PEC) water splitting provides an approach for realizing this conversion, by storing solar energy in hydrogen gas through an environmentally friendly process.[1–4] This process was first demonstrated in 1972 by Fujishima and Honda using titanium dioxide ($TiO_2$) as the photoanode.[5] Since this discovery, $TiO_2$ has been intensively studied for PEC water splitting because of its favorable band edge positions, resistance to photocorrosion, nontoxicity and low cost.[3,6–12]

Meanwhile, in addition to its optical absorption limitation within the ultraviolet region because of its large band gap, $TiO_2$ also suffers from rapid electron–hole recombination at the interface between the electrode and the electrolyte.[13–15] In this case, the surface state of $TiO_2$, primarily affecting the surface charge transfer efficiency, is critical for the PEC performance. To facilitate the surface charge transfer process, one strategy is to add a heterojunction layer, using materials with an upper valance band position compatible with that of $TiO_2$.[16–18] With the driving force from the upper junction layer, it is easier for the excited electron–hole pairs to be separated. Another approach, without considering the band position for guest materials, is to apply an oxygen evolution reaction (OER) co-catalyst layer.[19–21] The OER co-catalyst can dramatically improve the hole transfer from the photoanode to the electrolyte. In summary, a secondary overlayer on $TiO_2$ has been investigated to improve the PEC performance. However, an additional interface between $TiO_2$ and the overlayer will cause some efficiency loss owing to unmatched crystal structures.[22,23] For instance, as demonstrated by Yang's group, an epitaxial rutile shell had a positive effect on the PEC performance of rutile $TiO_2$ nanowires when compared with amorphous and anatase $TiO_2$ shells.[24]

In our previous research on the crystal engineering of Degussa P-25, the rutile phase in an anatase/rutile mixture phase was selectively disordered by a Li-EDA (Li dissolved in ethylenediamine) solution.[25] The disordered rutile phase facilitated the electron/hole separation, and we observed the effective transfer of holes from the photoanode to the electrolyte. In this work, *via* the excellent reductive ability of the Li-EDA solution, one-dimensional vertically aligned $TiO_2$ nanotube arrays grown on an FTO substrate, originally serving as a host with good charge transport properties because of their longitudinal direction[26–29] and large effective surface area benefiting the PEC performance, were modified to have an ultra-thin disordered overlayer shell.[30,31] The as-synthesized $TiO_2$ nanorod arrays on an FTO substrate were converted into nanotube structures *via* the chemical etching method, and a disordered overlayer was formed on the surface of the photoanode by treatment with the Li-EDA solution to facilitate the hole transfer process for more efficient water oxidation. A fabrication schematic diagram is shown in Fig. S1 (ESI†). By adjusting the treatment conditions in terms of time and solution concentration, optimized $TiO_2$ nanotube photoanodes can be obtained for efficient PEC water splitting.

Typical top and cross-sectional FE-SEM images of the $TiO_2$ nanorods fabricated by the hydrothermal method are shown in Fig. 1a and b. The nanorods are dense and vertically aligned with a square facet of approximately 100 to 200 nm and a length of approximately 4.7 μm. After the $TiO_2$ nanorods were etched with the acidic solution, $TiO_2$ nanotubes were obtained (Fig. 1c and d).

[a] *School of Chemical Engineering and SKKU Advanced Institute of Nanotechnology, Sungkyunkwan University, Suwon 440-746, Republic of Korea*
[b] *Department of Chemical and Biomolecular Engineering, Yonsei University, 50 Yonsei-ro, Seodaemun-gu, Seoul 120-749, Republic of Korea. E-mail: lutts@yonsei.ac.kr*
[c] *The 4th R&D Institute, 1st Directorate, Agency for Defense Development, Yuseong P.O. Box, Daejeon, 34186, Republic of Korea*

† Electronic supplementary information (ESI) available. See DOI: 10.1039/c6cc07611d

‡ These authors contributed equally to this work.

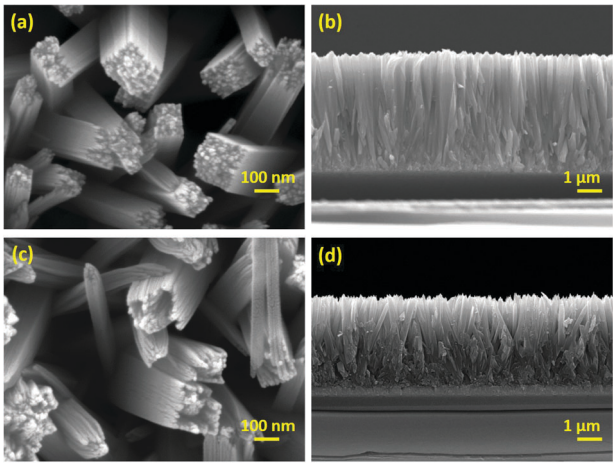


Fig. 1 Top-view SEM images of (a) $TiO_2$ nanorods and (c) $TiO_2$ nanotubes. Cross-sectional SEM images of (b) $TiO_2$ nanorods and (d) $TiO_2$ nanotubes.

The dissolution rate of $TiO_2$ in the etching solution along the axial direction is faster than along the side wall direction, resulting in an open-ended structure.[32] In this case, cavities can be observed from the surface of the rectangular $TiO_2$ nanotubes from the etching process, and the length of the formed nanotube was shorter (3.6 μm) than that of the original nanorod (4.7 μm). The wall thickness of the nanotubes can be estimated from Fig. 1 and Fig. S2 (ESI†) and is approximately 30 nm. After further treatment with the Li-EDA solution for different times and at various Li concentrations, no notable morphological changes were observed, which was confirmed by SEM observations, as shown in Fig. S3 and S4 (ESI†). In addition, no damage was observed in the nanotube structure after the Li-EDA treatment, illustrating its influence on only the disordering of the crystal structure.

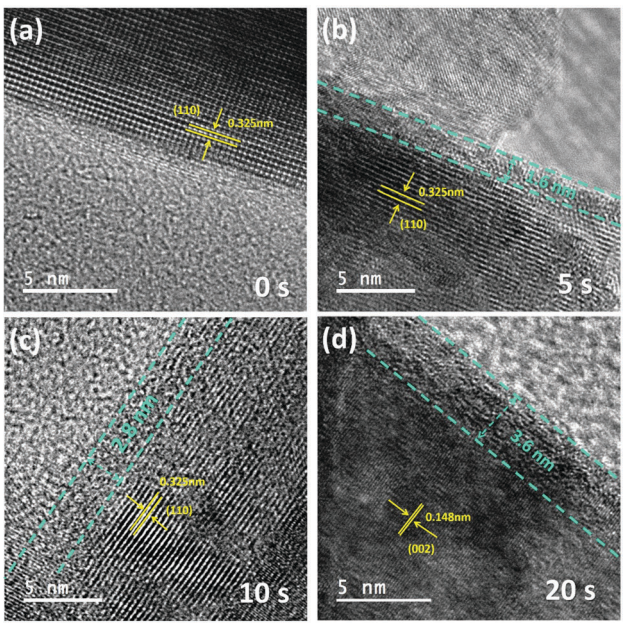


Fig. 2 TEM images of $TiO_2$ nanotubes treated with a 0.1 M Li-EDA solution for different durations: 0 s, 5 s, 10 s and 20 s.

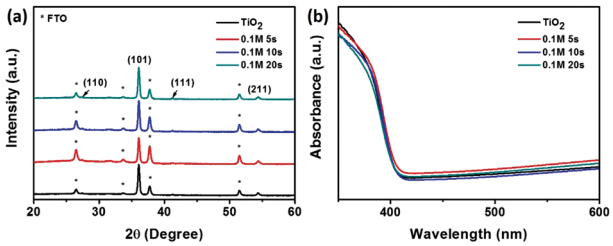


Fig. 3 (a) XRD spectra and (b) UV-vis absorption spectra of $TiO_2$ nanotubes treated with a 0.1 M Li-EDA solution for different durations: 0 s, 5 s, 10 s and 20 s.

To confirm this finding, a TEM investigation was conducted, as shown in Fig. 2, in which the surface crystal structures of the $TiO_2$ nanotubes were disordered by the Li-EDA treatment and could be easily distinguished from the rutile phase with a certain lattice constant. The thickness of the disordered layer increased according to the treatment time. By adjusting the concentration of the Li-EDA solution, the thickness of the disordered layer also shows similar regularity (Fig. S5, ESI†). The thickness values are illustrated in Fig. S6 (ESI†).

As the crystal structure of rutile $TiO_2$ cannot be well defined by TEM images, X-ray diffraction (XRD) spectra were recorded for samples with and without treatment in the Li-EDA solution (Fig. 3a). The XRD data showed peaks centered at 27.40°, 36.05°, 41.29°, and 54.38°, which, respectively, correspond to the (110), (101), (111), and (211) diffraction peaks of rutile $TiO_2$ (JCPDS No. 21-1276); the peaks labelled by asterisks represent the FTO phase. Because of the very low thickness of the disordered layer on the rutile nanotubes, no notable changes were observed between the samples with and without the Li-EDA solution treatment, which may be indicative of the disordered state on the surface of the treated samples. To evaluate the thin disordered layer, the influence of the disordered layer on the light absorption ability of the $TiO_2$ nanotubes was also investigated (Fig. 3b). In the UV-vis absorption spectra, no observable absorption behavior changes were found owing to the introduction of the disordered layer.

The surface state of the Li-EDA-treated $TiO_2$ nanotubes was confirmed by X-ray photoelectron spectroscopy (XPS), as shown in Fig. 4. The Ti 2p peaks gradually shifted to lower binding energies with increasing Li-EDA treatment time (Fig. 4a). These results may be ascribed to the unsaturated ionic bond of O–Ti, in agreement with reduced $TiO_2$ cases.[33] In the O 1s spectra (Fig. 4b), an increase in the negative shift of binding energy with longer Li-EDA treatment time indicates more oxygen vacancies compared with pristine $TiO_2$ nanotubes, resulting from electrons being transferred to the neighboring oxygen vacancies.[34] The results imply that the Li-EDA treatment gives rise to an intrinsic electronic structure change, which is likely due to the disordered surface layer. The valence band (VB) XPS spectra were also recorded, as shown in Fig. 4c–f, showing that the VB maxima of the $TiO_2$ nanotubes treated with the Li-EDA solution for 0 s, 5 s, 10 s and 20 s are 1.97 eV, 1.95 eV, 1.90 eV and 1.85 eV, respectively. The upshift of the VB position is closely related to the disordered layer thickness, which can be considered as a VB offset between

 

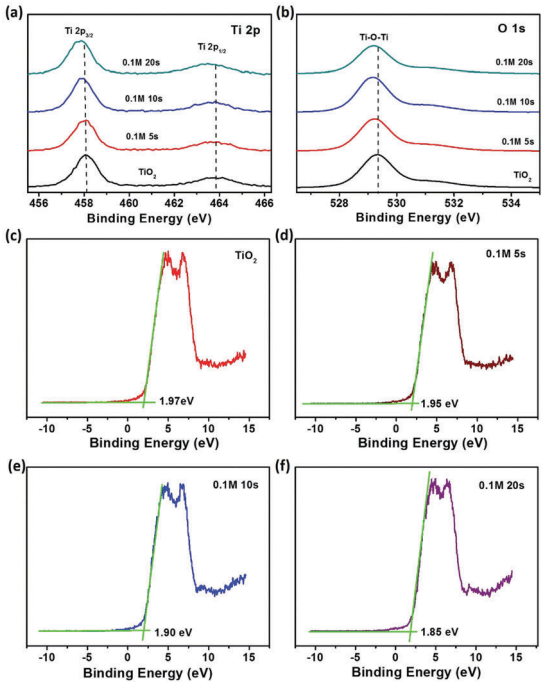


Fig. 4 (a) Ti 2p, (b) O 1s and (c–f) valence band XPS spectra of $TiO_2$ nanotubes treated with a 0.1 M Li-EDA solution for different durations: 0 s, 5 s, 10 s and 20 s.

the ordered region and the disordered region. According to our previous report, the fully disordered rutile $TiO_2$ has a maximum VB position upshift of 2.22 eV.[25] Therefore, the high carrier injection ratio properties lead to a VB offset that lies in the middle of the VB positions for ordered and disordered $TiO_2$. As a result, the upshift of the VB position may cause photogenerated holes to be efficiently transferred from the inner $TiO_2$ to the outer disordered layer.

To illustrate the above analyses, photocurrent density *vs.* potential (*J*–*V*) curves, reflecting the PEC ability of the $TiO_2$ photoanodes, are shown in Fig. 5 and Fig. S7 (ESI†). In the photocurrent densities, all of the samples treated with Li-EDA solution show enhanced PEC abilities, illustrating the effect of the disordered overlayer. By comparing different treatment times and solution concentrations, the optimized conditions were found to be 0.1 M and 10 s. The $TiO_2$ nanotubes treated under these conditions yielded a maximum photocurrent density value of 1.75 mA $cm^{-2}$ at 1.23 V *vs.* RHE, which is approximately

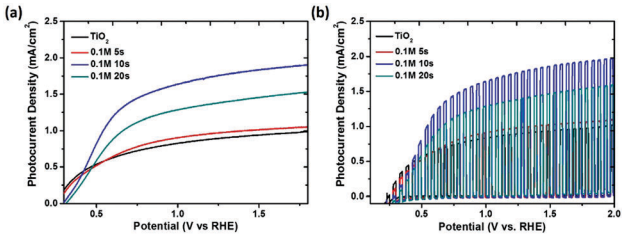


Fig. 5 (a) Linear and (b) chopped photocurrent–potential (*J*–*V*) curves of $TiO_2$ nanotubes treated with a 0.1 M Li-EDA solution for different durations: 0 s, 5 s, 10 s and 20 s.

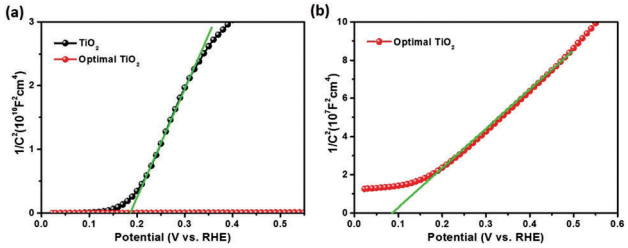


Fig. 6 (a) Mott–Schottky plots of pristine $TiO_2$ and $TiO_2$ optimally treated with a Li-EDA solution. (b) Amplified Mott–Schottky plots of $TiO_2$ optimally treated with a Li-EDA solution.

two times that of the pristine $TiO_2$ nanotubes. The thickness of the disordered layer for the optimal sample was 2.8 nm, illustrating that a thinner overlayer may not achieve the maximum contribution while a thicker overlayer may reduce the transfer efficiency. In addition, the PEC performances of the $TiO_2$ nanorods with and without Li-EDA treatment were also measured for comparison (Fig. S8, ESI†), illustrating the advantages of the open-ended structure.

Electrochemical impedance measurements were carried out to further investigate the effect of the disordered layer on the $TiO_2$ nanotubes treated with a Li-EDA solution. Fig. 6 shows the Mott–Schottky plots of the pristine $TiO_2$ nanotubes and $TiO_2$ nanotubes treated with the optimal Li-EDA solution. A Mott–Schottky analysis was performed in the dark to find the flat band potential, $V_{fb}$, and the donor concentration, $N_d$. The donor densities can be calculated by utilizing the slope of the Mott–Schottky plot through the following equation:

$$N_d = \frac{2}{\varepsilon\varepsilon_0 e_0}\left[d\left(1/C^2\right)/dV\right]^{-1}$$

where $N_d$ is the donor density, $e_0$ is the electron charge, $\varepsilon$ is the dielectric constant of $TiO_2$ ($\varepsilon$ = 83),[35] $\varepsilon_0$ is the permittivity of vacuum, and $V$ is the applied potential. The two $TiO_2$ samples showed a positive slope in the Mott–Schottky plots, which is characteristic of an n-type semiconductor.[33] The decrease in the slope indicates that the donor densities increased, as shown in the above equation.[36] The calculated donor densities of pristine $TiO_2$ and $TiO_2$ treated under optimal conditions were $1.01 \times 10^{19}$ $cm^{-3}$ and $8.02 \times 10^{21}$ $cm^{-3}$, respectively. The donor density increased by three orders of magnitude because of the oxygen vacancies that serve as electron donors, which would enhance the charge transfer and electrical conductivity, *i.e.*, two crucial contributions to the photocurrent density. In addition, the flat band potential for the $TiO_2$ nanotubes treated with the Li-EDA solution shifted cathodically from 0.18 V to 0.09 V *vs.* RHE, suggesting an upward shift of the Fermi level. This negative shift facilitates charge separation at the semiconductor–electrolyte interface by increasing the degree of band bending at the $TiO_2$ surface.

Based on the above analyses, a diagram of the working process for the $TiO_2$ disordered overlayer is shown in Fig. 7a. With the outer driving force for pushing holes and the improved interface charge transfer properties, the charge separation efficiency at the semiconductor–electrolyte interface can be enhanced. For further

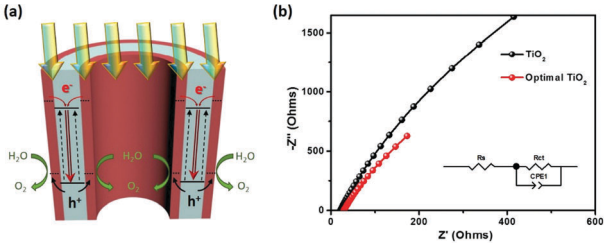


Fig. 7 (a) Illustration of the energy levels and charge transfer in Li-EDA-treated $TiO_2$ nanotubes. (b) EIS responses of $TiO_2$ and $TiO_2$ treated with a Li-EDA solution measured in 1 M NaOH at 1.23 V *vs.* RHE. The responses are recorded as Nyquist plots. The inset shows an equivalent circuit.

demonstration, electrochemical impedance spectra were recorded as Nyquist plots at 1.23 V *vs.* RHE in 1 M NaOH under 100 mW $cm^{-2}$ illumination (Fig. 7b). The inset shows the diagram of an equivalent circuit, and the $R_{ct}$ value is given in Table S1 (ESI†). The $R_{ct}$ value for pristine $TiO_2$ nanotubes is 16 489 Ohms, whereas the value for the $TiO_2$ nanotubes treated under optimal conditions is 9521 Ohms. As the $R_{ct}$ value signifies the charge transfer resistance at the photoanode–electrolyte interface, the overlayer decreases that resistance, corresponding to facilitation of the surface charge transfer process.

In conclusion, vertically aligned rutile $TiO_2$ nanotube arrays, with good charge transport properties and a large effective surface area, are a good candidate for disordered overlayer engineering to improve PEC performance. The optimally modified $TiO_2$ photoanodes produced a photocurrent density of up to 1.75 mA $cm^{-2}$ at 1.23 V *vs.* RHE. This result can be attributed to the enhanced surface charge transfer efficiency achieved with the assistance of a uniformly generated disordered overlayer, partially resulting from the open structure of the vertically aligned nanotube arrays. Further performance improvements can be expected by optimizing the length of the nanotube arrays. We believe that this simple processing method will further enable broad applications of photocatalytic materials.

This work was supported in part by the Yonsei University. Future-leading Research Initiative of 2015(2015-22-0067). This work was partially supported by the NRF of Korea Grant funded by the Ministry of Science, ICT and Future Planning (NRF-2013R1A2A1A09014038, 2015M1A2A2074663, C1 Gas Refinery Program (2016M3D3A1A01913254)).

## Notes and references

1 F. E. Osterloh, *Chem. Soc. Rev.*, 2013, **42**, 2294.
2 T. Hisatomi, J. Kubota and K. Domen, *Chem. Soc. Rev.*, 2014, **43**, 7520.
3 C. Acar and I. Dincer, *Int. J. Hydrogen Energy*, 2016, **41**, 7950.
4 K. Sivula and R. van de Krol, *Nat. Rev. Mater.*, 2016, 15010.
5 A. Fujishima and K. Honda, *Nature*, 1972, **238**, 37.
6 X. Chen, S. Shen, L. Guo and S. S. Mao, *Chem. Rev.*, 2010, **110**, 6503.
7 S. V. Awate, S. S. Deshpande, K. Rakesh, P. Dhanasekaran and N. M. Gupta, *Phys. Chem. Chem. Phys.*, 2011, **13**, 11329.
8 J. Yu, L. Qi and M. Jaroniec, *J. Phys. Chem. C*, 2010, **114**, 13118.
9 X. Liu, J. Li, Y. Zhang and J. Huang, *Chem. – Eur. J.*, 2015, **21**, 7345.
10 Y. Luo, X. Liu and J. Huang, *CrystEngComm*, 2013, **15**, 5586.
11 G. Liu, X. Yan, Z. Chen, X. Wang, L. Wang, G. Q. Lu and H. Cheng, *J. Mater. Chem.*, 2009, **19**, 6590.
12 Y. K. Kho, A. Iwase, W. Y. Teoh, L. Madler, A. Kudo and R. Amal, *J. Phys. Chem. C*, 2010, **114**, 2821.
13 M. Ni, M. K. H. Leung, D. Y. C. Leung and K. Sumathy, *Renewable Sustainable Energy Rev.*, 2007, **11**, 401.
14 Y. Li and J. Z. Zhang, *Laser Photonics Rev.*, 2010, **4**, 517.
15 M. G. Walter, E. L. Warren, J. R. McKone, S. W. Boettcher, Q. X. Mi, E. A. Santori and N. S. Lewis, *Chem. Rev.*, 2010, **110**, 6446.
16 H. Kim, D. Monllor-Satoca, W. Kim and W. Choi, *Energy Environ. Sci.*, 2015, **8**, 247.
17 Y. Lee, C. Chi and S. Liau, *Chem. Mater.*, 2010, **22**, 922.
18 Y. Pu, G. Wang, K. Chang, Y. Ling, Y. Lin, B. C. Fitzmorris, C. Liu, X. Lu, Y. Tong, J. Z. Zhang, Y. Hsu and Y. Li, *Nano Lett.*, 2013, **13**, 3817.
19 G. Wang, X. Xiao, W. Li, Z. Lin, Z. Zhao, C. Chen, C. Wang, Y. Li, X. Huang, L. Miao, C. Jiang, Y. Huang and X. Duan, *Nano Lett.*, 2015, **15**, 4692.
20 M. Ma, J. K. Kim, K. Zhang, X. Shi, S. J. Kim, J. H. Moon and J. H. Park, *Chem. Mater.*, 2014, **26**, 5592.
21 M. Ma, X. Shi, K. Zhang, S. Kwon, P. Li, J. K. Kim, T. T. Phu, G. Yi and J. H. Park, *Nanoscale*, 2016, **8**, 3474.
22 T. Li, J. He, B. Pena and C. P. Berlinguette, *Angew. Chem., Int. Ed.*, 2016, **55**, 1769.
23 M. Ma, K. Zhang, P. Li, M. S. Jung, M. J. Jeong and J. H. Park, *Angew. Chem., Int. Ed.*, 2016, **55**, 11819.
24 Y. J. Hwang, C. Hahn, B. Liu and P. Yang, *ACS Nano*, 2012, **6**, 5060.
25 K. Zhang, L. Wang, J. K. Kim, M. Ma, G. Veerappan, C. Lee, K. Kong, H. Lee and J. H. Park, *Energy Environ. Sci.*, 2016, **9**, 499.
26 A. I. Hochbaum and P. Yang, *Chem. Rev.*, 2010, **110**, 527.
27 N. S. Lewis, *Science*, 2007, **315**, 798.
28 K. Shankar, J. I. Basham, N. K. Allam, O. K. Varghese, G. K. Mor, X. Feng, M. Paulose, J. A. Seabold, K.-S. Choi and C. A. Grimes, *J. Phys. Chem. C*, 2009, **113**, 6327.
29 C. M. Lopez and K.-S. Choi, *Chem. Commun.*, 2005, 3328.
30 J. H. Park, S. Kim and A. J. Bard, *Nano Lett.*, 2006, **6**, 24.
31 P. Roy, S. Berger and P. Schmuki, *Angew. Chem., Int. Ed.*, 2011, **50**, 2904.
32 L. Liu, J. Qian, B. Li, Y. Cui, X. Zhou, X. Guo and W. Ding, *Chem. Commun.*, 2010, **46**, 2402.
33 Q. Kang, J. Cao, Y. Zhang, L. Liu, H. Xu and J. Ye, *J. Mater. Chem. A*, 2013, **1**, 5766.
34 I. S. Cho, J. Choi, K. Zhang, S. J. Kim, M. J. Jeong, L. Cai, T. Park, X. Zheng and J. H. Park, *Nano Lett.*, 2015, **15**, 5709.
35 S. K. Kim, W. Kim, K. Kim, C. S. Hwang and J. Jeong, *Appl. Phys. Lett.*, 2004, **85**, 4112.
36 K. Rajeshwar, Fundamentals of Semiconductor Electrochemistry and Photoelectrochemistry, *Encyclopedia of Electrochemistry*, Wiley-VCH, Weinheim, Germany, 2002.



 